Photo-induced high-temperature order-disorder phase transition in $CaSnO_3$ perovskite revealed by Raman spectroscopy.

C.-J. Chen[1], J. Kung[1], C.-M. Lin[2], M. Zhang[3], S.A.T. Redfern[3§]

1. Department of Earth Sciences, National Chen Kung University, 1 University Road, 701 - Tainan, Taiwan

2. Department of Applied Science, National Hsinchu University, 300 - Hsinchu, Taiwan

3. Department of Earth Sciences, University of Cambridge, Downing Street, Cambridge, CB2 3EQ, U.K.

§ e-mail: satr@cam.ac.uk

Abstract

Calcium stannate perovskite ($CaSnO_3$) has been studied by Raman spectroscopy at two excitation wavelengths (514.5 nm and 632.8 nm). A new first-order order-disorder phase transition induces Raman frequency shifts and line width doubling at 121˚C on heating (94˚C on cooling), seen in experiments using the 514.5 nm line of an Ar^+-ion laser. The transition is also seen when using a 623.8 nm He-Ne laser and by differential scanning calorimetry (DSC), but without strong order-disorder character, indicating that the phase transition is dependent on photo-excitation. High-temperature powder X-ray diffraction measurements provide thermal expansion coefficients of $\alpha_x = 13.9 \times 10^{-6}$ K^{-1}, $\alpha_y = 2.7 \times 10^{-6}$ K^{-1}, $\alpha_z = 14.3 \times 10^{-6}$ K^{-1}. The phase transition is postulated to be associated with photo-excited charged and conductive nanoscale ferroelectric order-disorder. As such, $CaSnO_3$ could represent the first in a new class of optoelectronic materials with additional potential photocatalytic properties.

1. Introduction

Calcium stannate is a member of the perovskite family of materials, alongside other alkaline earth stannates. The structures of the alkaline earth stannates were first determined by Megaw [1] and, at room temperature, range from cubic *Pm*3*m* [2] (for $BaSnO_3$) to

orthorhombic *Pnma* (sometimes referred to in the equivalent space group setting as *Pbnm*) [3] (in the case of $CaSnO_3$) accompanied by increasing tilting of the stannate octahedra, as discussed by Mountstevens et al. [4]. The stannate perovskites, examples of strongly correlated electron systems, are typically thought of as wide bandgap semiconductors. Their electronic structure was studied by Mizoguchi et al. [5] and Zhang et al. [6] who reported that the lowest energy states in the conduction band are associated with the interaction between the antibonding tin 5s and the oxygen 2p orbitals. The conduction bandwidth decreases strongly in response to the increasing octahedral tilting distortion, leading to an increase in the direct band gap from 3.1 eV in $BaSnO_3$ to 4.4 eV in $CaSnO_3$ [5, 6]. However, it has further been suggested, in the basis of ab initio calculations, that Fe-doped $CaSnO_3$ may show semi-metallic properties and represent a new class of spintronic materials [7]. Furthermore, Bannikov et al. [8] have also indicated that $SrSnO_3$ might be expected to show the characteristics of a magnetic semiconductor upon O-site doping by non-magnetic 2p elements.

The earliest reference to the use of alkaline earth stannates is in old English colour formulas which refer to the use of calcium stannate in compounding chrome tin reds [9]. More recently, there has been considerable interest in the alkaline earth stannates from both a microelectronics device point of view [9] (as thermally-stable capacitor dielectrics, due principally to their low-temperature-dependence of dielectric susceptibility between room temperature and 300˚C [10]) and for nano-ferroelectric properties and relaxor phenomena which become important as the structure approaches the cubic aristotype at high temperature [11, 12]. Potential uses in humidity sensors, catalytic converters, photocatalysis and batteries have also been highlighted. In addition $CaSnO_3$ has attracted the attention of the geophysics community [13, 14], because it is an isostructural analogue of $(Mg,Fe)SiO_3$ perovskite (the most abundant silicate mineral in Earth). Computer simulation of high pressure stabilities of $CaSnO_3$ suggested a phase transition from perovskite to the $CaIrO_3$-type post-perovskite

structure occurs occurring at ~ 12 GPa [15] although this is not confirmed by experimental investigations [16].

In common with the experimental observations of $CaSnO_3$ at high pressure, there are no reported phase transitions for $CaSnO_3$ at high temperature, and it is assumed to remain orthorhombic *Pnma* up to its melting point. Here, we report results of high-temperature Raman spectroscopy that indicate that the solid state temperature dependent properties of $CaSnO_3$ may be more complex than this initial picture suggests, and present evidence for a first-order photo-induced order-disorder phase transition above room temperature.

2. Experiments

The $CaSnO_3$ sample studied here was prepared by a solid state reaction method, employing a 1:1 molar mixture of $CaCO_3$ and SnO_2 which was then sintered at 1200˚C in air at atmospheric pressure for 20 hours. This resulted in a well-crystallized homogeneous powder that was confirmed as *Pnma* orthorhombic $CaSnO_3$ perovskite by X-ray powder diffraction. This sample was subsequently studied by Raman spectroscopy, infrared spectroscopy and X-ray diffraction as a function of temperature up to beyond 200˚C.

Two sets of Raman spectroscopic experiments were performed. In the first, Raman-scattering data were obtained using the 514.5 nm line of a Spectra-Physics *Stabilite* 2017 Ar^+ ion laser with 0.6 W power focused to about 2 ~ 4 μm spot diameter at the sample surface. The measurements were performed with a micro-Raman option using a Jobin-Yvon Spex Spectrum One liquid N_2–cooled charge-coupled device (CCD). The Raman signal was analyzed by employing normal backscattering geometry with a Leitz UM 32 microscope objective with 600 seconds integration time. Scattered light dispersed by the spectrometer was detected by the CCD. The spectral resolution was typically better than 1 cm^{-1}. A

microscope–compatible thermal stage was used while recording the temperature-dependent spectra from 30 to 1070˚C over a range of frequencies from 100 to 1300cm^{-1} .

A subsequent set of Raman experiments were performed using a Jobin-Yvon LabRam 300 instrument with a 632.8 nm, 20 mW He-Ne laser backscattered from a 2μm-diameter spot with CCD collection (600 second accumulation time) in similar geometry to the first set of experiments, and over a similar range of frequencies and from room temperature to 200˚C.

In situ high-temperature X-ray diffraction data were collected on the same sample with a Bruker D8 Advance powder diffractometer, between 20° and 90° 2θ using CuKα_1 radiation in isothermal temperature steps of 10˚C from room temperature to 800˚C ramped between each accumulation at a rate of 0.5 ˚C/min.

The phase transition behavior in $CaSnO_3$ was analyzed by differential scanning calorimetry (DSC) using a Perkin Elmer Diamond DSC in high speed "hyper-DSC" mode [17]. Approximately 10 mg of $CaSnO_3$ powder was placed in an aluminum pan and measurements were carried out between room temperature and 600 ˚C at a heating rate of 40 ˚C min^{-1}. Cooling experiments were conducted at the same ramp rate.

Infrared absorption spectra were recorded as a function of temperature from room temperature to 250˚C under vacuum using a Bruker 113v Fourier transformation infrared (FTIR) instrument. Spectra were measured between 50 and 700 cm^{-1} at a resolution of 2 cm^{-1} using DTGS detector and 3.5μm Mylar beam splitter. The crystalline sample was thoroughly mixed with dry CsI dilutant to a ratio of 1:300 sample:CsI by mass. A 300mg, 13-mm diameter disc was prepared by pressing the mixture at 75MPa. A pure CsI disc was prepared in a similar manner and used as a reference for infrared measurements.

3. Results and analysis

3.1 High-temperature 514.5 nm laser Raman observations

Raman spectroscopy is sensitive to changes in structure and has been extensively used previously to investigate structural instabilities in perovskites. These typically result in changes in the frequencies and profiles of Raman modes as a function of temperature. Most recently Raman spectroscopy was used to demonstrate the existence of previously undiscovered phase transitions in $SrSnO_3$ [18, 19]. At room temperature the crystal structure of $CaSnO_3$ is assumed to be orthorhombic, point group *mmm* (D_{2h}) and space group *Pnma* (D_{2h}^{16}). As such, the Raman active modes for this *Pnma* structure are $\Gamma_{Raman} = 7A_g + 5B_{1g} + 7B_{2g} + 5B_{3g}$, which represent four antisymmetric and two symmetric octahedral stretching modes, four bending modes, and six octahedral rotation or tilt modes. The other eight modes are associated with the calcium cations. At room temperature, we find $CaSnO_3$ Raman modes at 164, 182, 225, 250, 264, 277, 356, 362, 443, 506, and 700 cm^{-1}, in good agreement with the previous room temperature studies of McMillan and Ross [20] and Tarrida et al. [21]. Following the work of Lin (personal communication) the three strongest sharp modes at 182, 277, 356 cm^{-1} can be assigned to A_g rotation modes. The remainder of the observed Raman modes are rather weak.

The temperature-dependence of the $CaSnO_3$ Raman spectrum was studied from 30 to 1070˚C measured between 100 and 1300 cm^{-1}. Here we focus on the behavior below 200˚C. During progressive heating the Raman spectra show strong temperature-dependent changes (Fig. 1) with peaks shifting discontinuously in a stepwise fashion to lower frequency at approximately 120˚C. The spectra obtained on cooling show that the modes recover to their original room temperature frequencies on cooling through at around 80˚C.

Raman profiles can be characterized by their peak frequencies ω_0 and line widths Γ_0, using appropriate functions fitted to the measured spectra. The temperature evolution of the

frequency of the measured bands is shown in Fig. 2 where one finds significant change in frequency at around 120˚C for five modes: those near 182, 277, 356, 443, and 700 cm^{-1}. The shift of the 182 cm^{-1} mode is 11 cm^{-1}, that of 277 is 15 cm^{-1}, 356 is 17 cm^{-1}, 433 is 9 $cm^{-1}$and 700 cm^{-1} is as much as 60 cm^{-1}. Such abrupt frequency shifts of up to 20 cm^{-1} of these A_g modes cannot simply be explained by thermal expansion. On cooling through the same temperature interval the modes recover to their original frequencies at around 80˚C, indicating a marked thermal hysteresis in the phenomenon. Concomitant with the changes in frequencies of these modes, we see significant changes in line widths, with the modes that show large frequency shifts also displaying significant and abrupt increases in line broadening on heating through 120˚C and decreasing abruptly back to the original room temperature line widths on cooling through 80˚C (Fig. 3). The widths at temperatures above the abrupt change are approximately twice the value below the change.

3.2 High-temperature 632.8 nm laser Raman observations

A further investigation of the phenomenon observed above was undertaken using a second Raman instrument, with a He-Ne exciting laser via a Jobin-Yvon LabRam instrument in similar geometry. We anticipated that we would obtain confirmatory results, but intriguingly the behavior seen using this arrangement differed significantly from that seen previously. While the room temperature data are comparable (Fig. 4) we find that the temperature-dependence of the Raman frequencies and line widths does not show the same step-wise anomalous characteristics on heating, with no abrupt shifts in frequencies or line widths in the regions where they are seen using the Ar^+-ion Raman set up (Fig. 5). Indeed, the temperature-dependent Raman spectra are rather continuous in character, but the frequencies of Raman modes do show a variation with temperature at around 120 ˚C on heating that could be interpreted as a second-order phase transition. Experiments were repeated using

both instruments, several times, to confirm these observations.

3.3 Differential Scanning Calorimetry

The DSC curve of CaSnO3 is shown on heating in figure 6. We note a small but clear anomaly in the rate of heat flow at 121 ˚C. The DSC measurement shows a stepwise decrease in heat flow at this temperature, apparently characteristic of a second-order phase transition. We see no evidence of a λ-anomaly or first-order behavior. However, background-subtracted data are shown in the inset, and reveal that the same transition is seen on cooling at 94 ˚C. These temperatures correspond to those at which the Raman active modes show anomalous frequency shifts, and confirm that these shifts are associated with thermodynamic transitions in the material.

3.4 Infrared and X-ray observations

The Fourier transform infrared (FTIR) spectrum of *Pnma* $CaSnO_3$ perovskite should contain twenty-five dipole active optic phonons, which can be subdivided as $9B_{1u} + 7B_{2u} + 9B_{3u}$. Line broadening due to phonon scattering and structural defects results in fewer phonon modes being experimentally distinguishable at (and above) room temperature. Our FTIR spectra show features similar to those seen in other *Pnma* perovskites [22]. On heating the infrared bands show no significant variations other than monotonic shifts in frequency and peak width (Fig. 7). This contrasts with the strong shifts or Raman lines seen in the Ar^+-ion Raman experiments and indicative of an order-disorder phase transition. We carried out further study of the structural evolution of $CaSnO_3$ perovskite in this temperature interval by X-ray diffraction (XRD). The powder diffraction patterns were refined using Rietveld methods to yield orthorhombic cell parameters as a function of temperature. The orthorhombic cell edges can be expressed in terms of pseudo-cubic equivalents, which would

be expected to converge to a single value in the cubic perovskite structure. Indeed, on heating we find that the cell parameters show some convergence, indicative of decreasing orthorhombic spontaneous strain on increasing temperature (Fig. 8). The projected phase transition, indicated by extrapolation of these trends to high temperature, lies well above the melting point of $CaSnO_3$. Data collected on cooling are identical, within experimental error, to the values obtained on heating. The thermal expansion is anisotropic with that along the crystallographic *x* and *z* axes approximately the same (α_x = 13.9 x 10^{-6} K-1, α_z = 14.3 x 10^{-6} K^{-1}) and the expansion along the *y* axis considerably smaller (α_y = 2.7 x 10^{-6} K^{-1}). There is no indication of any anomalous change in the cell parameters in the region of phase transitions suggested by the Raman and DSC measurements.

Discussion and conclusions

The results from Raman and DSC measurements indicate that a new structural phase transition has been found in calcium stannate at 121˚C (on heating) which reverses on cooling at 94˚C. When measured using the 514.5 nm line of an AR+-ion laser, the strong A_g Raman-active optical phonon modes exhibit anomalous frequency shifts at these temperatures, alongside a large increase in line widths (of the order of doubling in widths) on heating through the this temperature. The large increase in line width, the stepwise nature of the increase, and the hysterisis in properties would seem to indicate that there is a thermodynamically first-order order-disorder type phase transition in $CaSnO_3$.

The lack of any similar indication of a strongly first-order phase transition in the He-Ne laser Raman, DSC, FTIR and XRD experiments is, therefore, intriguing. We postulate that the photon energy of the Ar^+ ion laser itself is playing a role in the observed transformation behavior. The Ar^+ ion laser operated at higher power at the sample, but more importantly with

a photon energy of the 50 mW beam of the 514.5 nm Ar^+ ion laser is 2.41 eV while that of the 20 mW beam of the 632.8nm He-Ne laser is 1.96 eV. We can discount laser heating as a source of credible difference between the two Raman experiments since He-Ne laser Raman, FTIR and XRD measurements were carried out in each case to much higher temperatures with no evidence of transformation behavior up to the melting point. Furthermore, it may be that the collective transition occurs on a length scale that is shorter than the correlation length for X-ray diffraction, but still observable by Raman scattering.

The reported band gap for $CaSnO_3$, of 4.4 eV, remains significantly greater than the photon energy of the Ar^+ ion laser. However, we note that in $CaSnO_3$ at room temperature strong photoluminescence has been observed at a wavelength much longer than usually observed for oxides containing main group ions. Intrinsic charge transfer across the band gap is not expected under illumination by a 514.5 nm laser, but defects might well play a significant role in decreasing the effective gap. For example, Bannikov et al. [8] have recently shown that the substitutional introduction of non-magnetic impurities such as boron, carbon and nitrogen replacing oxygen in the perovskite lattice can lead to new impurity 2p bands localised in the intrinsic band gap; these impurity levels may split and lead to magnetic properties. While calculations have not be carried out for $CaSnO_3$, the study of $SrSnO_3$ showed that, in the stannate perovskite, carbon impurities on the oxygen sublattice lead to the development of a magnetic semiconductor [8]. Intermediate states similar to these impurity-related bands are likely to be responsible for the effects observed in our experiments, such that a photo-excited state lying at an energy $\leq$ 2.4 eV above the valence band may be obtained in our sample, as indicated by the different behaviour seen under 514.5nm and 632.8nm laser illumination.

Furthermore, on heating above 121˚C we find $CaSnO_3$ shows a transition whose nature is dependent upon photo excitation, as revealed by the 514.5nm laser Raman line

widths and frequencies. Similar behaviour has been noted for charge/order orbital order/disorder in manganite perovskites (Ogasawara, 2002), where a direct first order phase transition to a disordered state was observed as a photo-induced phenomenon. In $CaSnO_3$, the disordering process is also temperature-dependent. By analogy to the photo-induced ferroelectric phenomena seen in titanate perovskites (Nasu, 2004), and bearing in mind the recent observation (Goodwin, 2007) of ferroelectric nano-domain order-disorder at high temperature in $SrSnO_3$, one possibility is that the order-disorder transition seen at 121˚C by Raman spectroscopy has its origins in a nano-scale change in the ferroelectric order associated with local Sn displacements, dependent upon photo-excitation and temperature. In this case the origins of the transition would lie in the strong electron-phonon coupling typical of oxide perovskites, and the formation of super para-electric large polarons which then display a nano-ferroelectric order-disorder transition, first order in character. The fact that the large first-order characteristic of the transition is not seen in our other experiments is a consequence of its dependence on photo-stimulation.

In summary, we have shown that $CaSnO_3$, a known photoluminescent perovskite closely related to other known nano-ferroelectric perovskites, displays an order-disorder phase transition at 121˚C (on heating), with large temperature hysterisis and first order character upon photo-stimulation by light of 514.5nm wavelength. The transition is also seen, but with a more continuous character, when studied by DSC and lower energy Raman scattering. This high-temperature photo-induced collective structural change in $CaSnO_3$ warrants further investigation and may be associated with charged and conductive nano-scale ferroelectric domains. As such, $CaSnO_3$ could represent the first in a new class of optoelectronic materials with potential photocatalytic properties.

Acknowledgements

This study was supported by the UK Royal Society and the National Science Council of Taiwan in the form of a Joint Project grant to JK and SATR.

References

1. Megaw H D 1946 *Proc.Phys. Soc.* **58** 122

2. Hinatsu, Y. (1996) *Journal of Solid State Chemistry*, *122*, 384.

3. Vegas, A.; Valletregi, M.; Gonzalezcalbet, J. M.; Alariofranco, M. A. (1986) *Acta Crystallogr. Sect. B-Struct. Commun.*, *42*, 167.

4. Mountstevens, E. H.; Attfield, J. P.; Redfern, S. A. T. (2003) *Journal of Physics-Condensed Matter*, *15*, 8315.

5. Mizoguchi, H.; Woodward, P. M. (2004) *Chem. Mat.*, *16*, 5233.

6. Zhang, W. F.; Tang, J.; Ye, J. (2006) *Chem Phys Lett, 418*, 174

7. Shein, I. R.; Kozhevnikov, V. L.; Ivanovskii, A. L. (2006) *Semiconductors*, *40*, 1261.

8. Bannikov, V. V.; Shein, I. R.; Kozhevnikov, V. L.; Ivanovskii, A. L. (2008) *Journal of Magnetism and Magnetic Materials*, *320*, 936.

9. Coffeen, W.W. (1953) J Am. Ceram. Soc. 36, 207.

10. Azad, A. M.; Shyan, L. L. W.; Alim, M. A. (1999) *Journal of Materials Science*, *34*, 3375.

11. Mountstevens, E. H.; Redfern, S. A. T.; Attfield, J. P. (2005) *Physical Review B*, *71*.

12. Goodwin, A. L.; Redfern, S. A. T.; Dove, M. T.; Keen, D. A.; Tucker, M. G. (2007) *Physical Review B*, *76* #174114

13. Zhao, J.; Ross, N. L.; Angel, R. J. (2004) *Physics and Chemistry of Minerals*, *31*, 299.

14. Kung, J.; Angel, R. J.; Ross, N. L. (2001) *Physics and Chemistry of Minerals*, *28*, 35.

15. Tsuchiya, T.; Tsuchiya, J. (2006) *American Mineralogist*, *91*, 1879.

16. Schneider, B. W.; Liu, W.; Li, B. S. (2008) *High Pressure Research*, *28*, 397.

17. Saunders, M.; Podluii, K.; Shergill, S; Buckton, G.; Royall P. (2004) *International Journal of Pharmaceutics*, 274, 35-40

18. Singh, M. K.; Karan, N. B.; Katiyar, R. S.; Scott, J. F.; Jang, H. M. (2008) *Journal of Physics – Condensed Matter* 20, 055210

19. Singh, M. K., Hong, J. W., Karan, N. K., Jang, H. M., Katiyar, R. S., Redfern, S. A. T., Scott, J. F. (2010) *Journal of Physics – Condensed Matter, accepted for publication*.

20. McMillan, P.; Ross, N. (1988) *Physics and Chemistry of Minerals*, *16*, 21.

21. Tarrida, M.; Larguem, H.; Madon, M. (2009) *Physics and Chemistry of Minerals*, *36*, 403.

22. Sopracase, R.; Gruener, G.; Olive, E.; Soret, J. C. (2010) *Physica B-Condensed Matter*, *405*, 45.

23. Nasu, K. (2004) *Reports on Progress in Physics*, *67*, 1607.

24. Ogasawara, T.; Tobe, K.; Kimura, T.; Okamoto, H.; Tokura, Y. (2002) *Journal of the Physical Society of Japan*, *71*, 2380.

Figure Captions

Figure 1: Raman spectra of $CaSnO_3$ excited by a 514.5nm laser, collected on heating and cooling between 25 and 200˚C. Individual spectra are offset vertically for clarity.

Figure 2: Temperature evolution of frequency shifts of three selected Raman modes. An abrupt frequency shift is observed at 120˚C on heating and 85˚C on cooling, which indicats a thermal hysteresis in the phenomenon. The selected Raman modes shown here are the three strongest modes for $CaSnO_3$ perovskite; 182 cm^{-1}, 277 cm^{-1} and 356 cm^{-1}.

Figure 3: The line width of Raman modes changes across the temperatures associated with the abrupt frequency shift shown in Fig. 2. The selected Raman modes shown here are the same as shown in Fig. 2.

Figure 4: Room temperature Raman spectra of $CaSnO_3$ perovskite collected using two different laser excitation sources of 514.5 nm and 632.8 nm.

Figure 5: Comparisons of temperature evolution of frequency shifts (a) and line width change (b) collected with two different laser excitation sources of 514.5 nm and 632.8 nm across the temperature range from 30 ˚C to 200˚C.

Figure 6: Differential thermal calorimetry (DSC) of $CaSnO_3$ on heating between 60 and 200˚C (endothermic up). Note the step in heat flow at the phase transition on heating at 121˚C. The inset shows the background-subtracted heat flow for heating and cooling, revealing the reverse transformation on cooling through 94˚C.

Figure 7: FTIR spectra collected on the heating from room temperature to 250˚C. There are no significant changes observed in frequency shift and peak width.

Figure 8: Temperature evolution of the cell parameter of $CaSnO_3$ perovskite expressed in terms of pseudo-cubic symmetry.

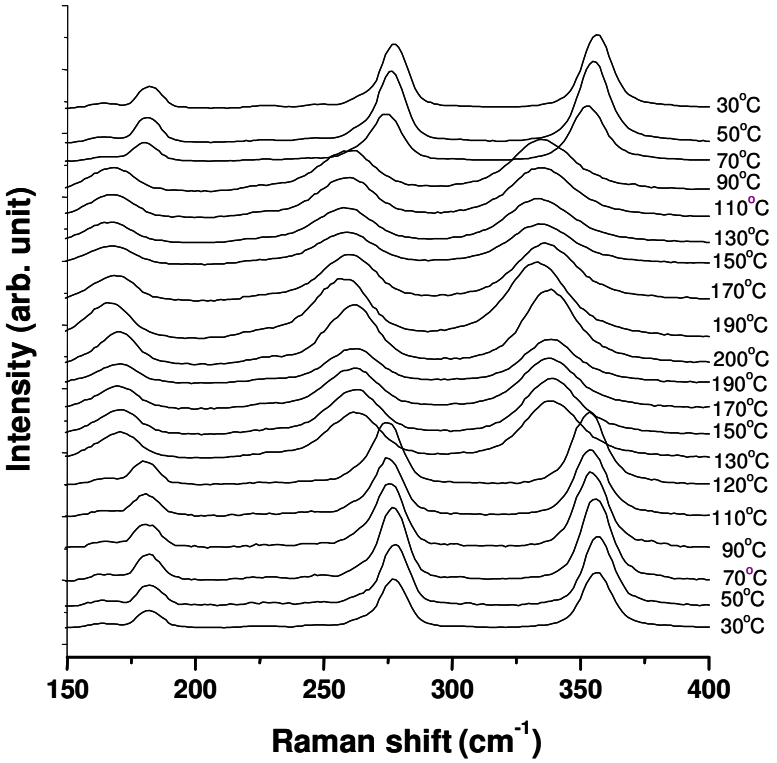
Intensity (arb. unit)
Raman shift (cm-1)
150
200
250
300
350
400
30°C
50°C
70°C
90°C
110°C
130°C
150°C
170°C
190°C
200°C
190°C
170°C
150°C
130°C
120°C
110°C
90°C
70°C
50°C
30°C

Fig. 1

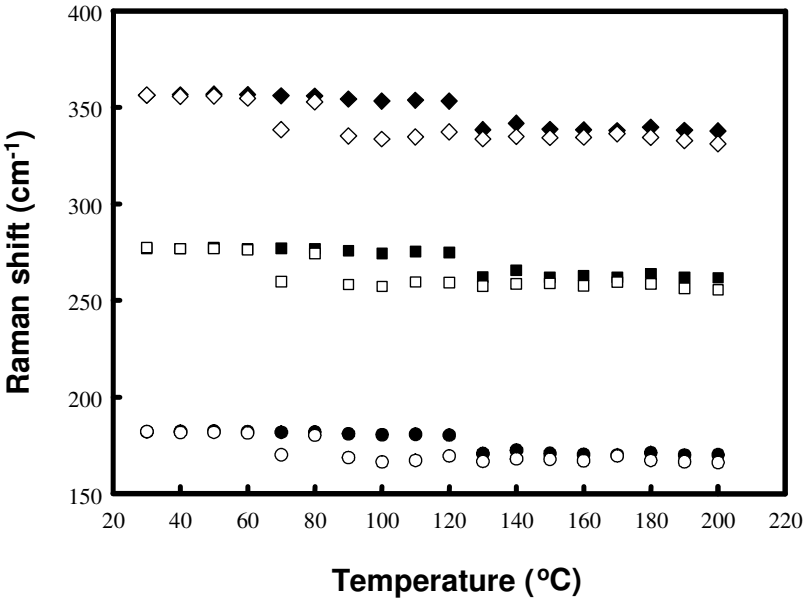
400
350
300
250
200
150
20
40
60
80
100
120
140
160
180
200
220
Raman shift (cm-1)
Temperature (ºC)

Fig. 2

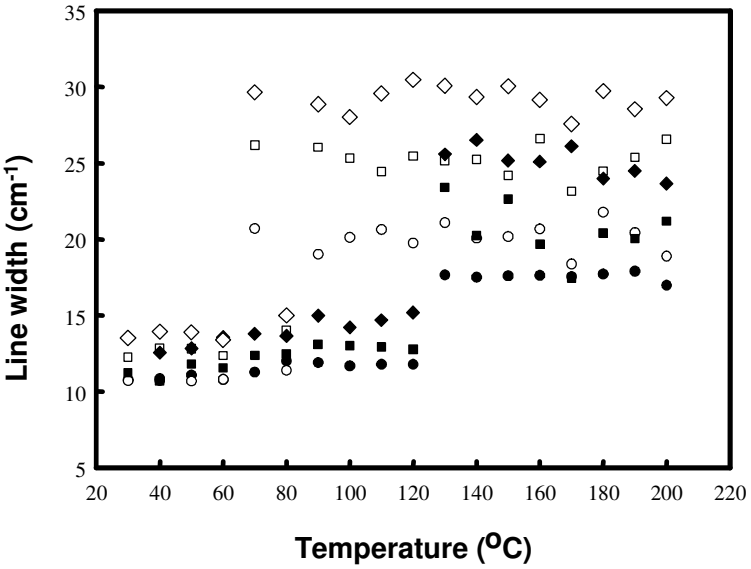
Line width (cm-1)
35
30
25
20
15
10
5
20
40
60
80
100
120
140
160
180
200
220
Temperature (OC)

Fig. 3

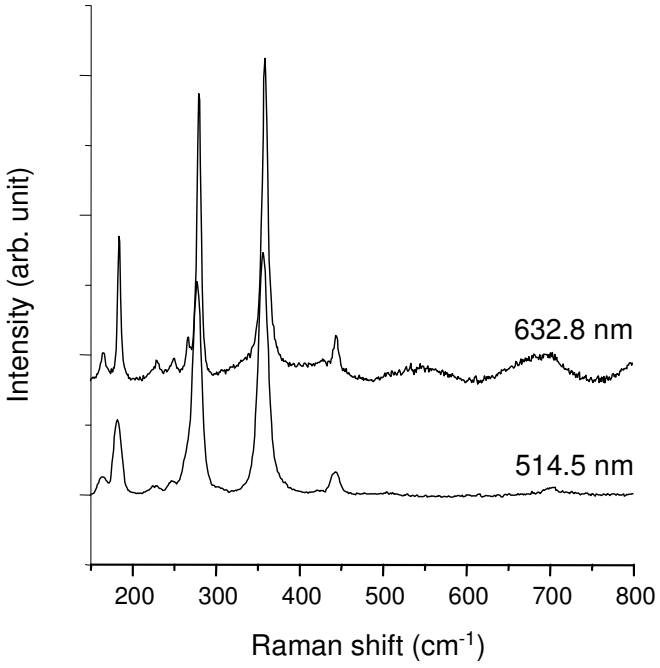
Intensity (arb. unit)
632.8 nm
514.5 nm
200
300
400
500
600
700
800
Raman shift (cm-1)

Fig. 4

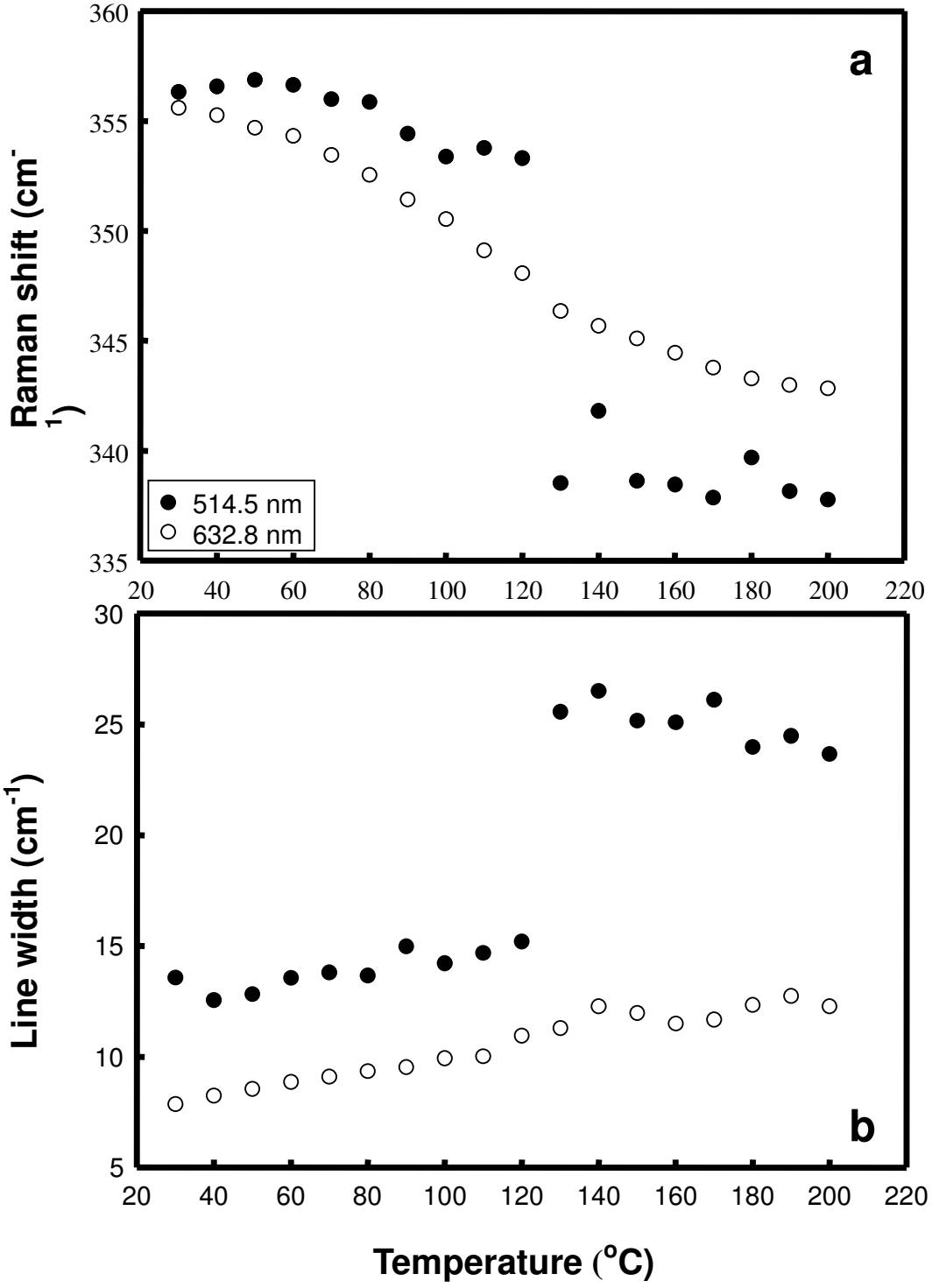
a
b
514.5 nm
632.8 nm
Raman shift (cm-1)
Line width (cm-1)
Temperature (°C)

Fig. 5

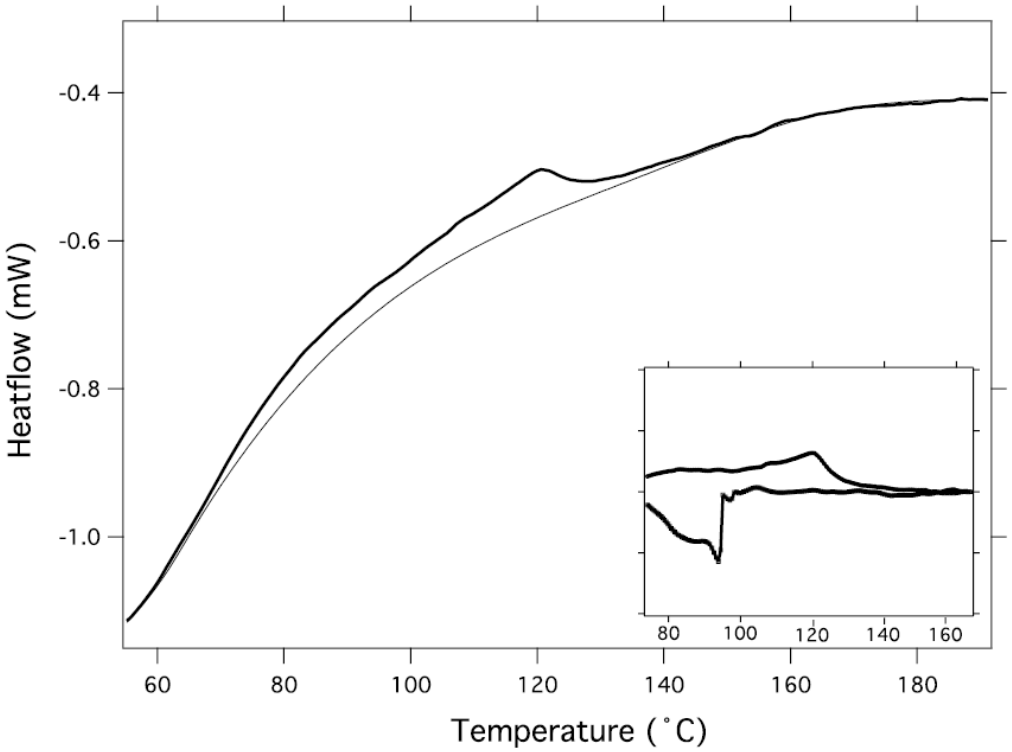
-0.4
-0.6
-0.8
-1.0
Heatflow (mW)
60
80
100
120
140
160
180
Temperature (˚C)
80
100
120
140
160

Fig 6

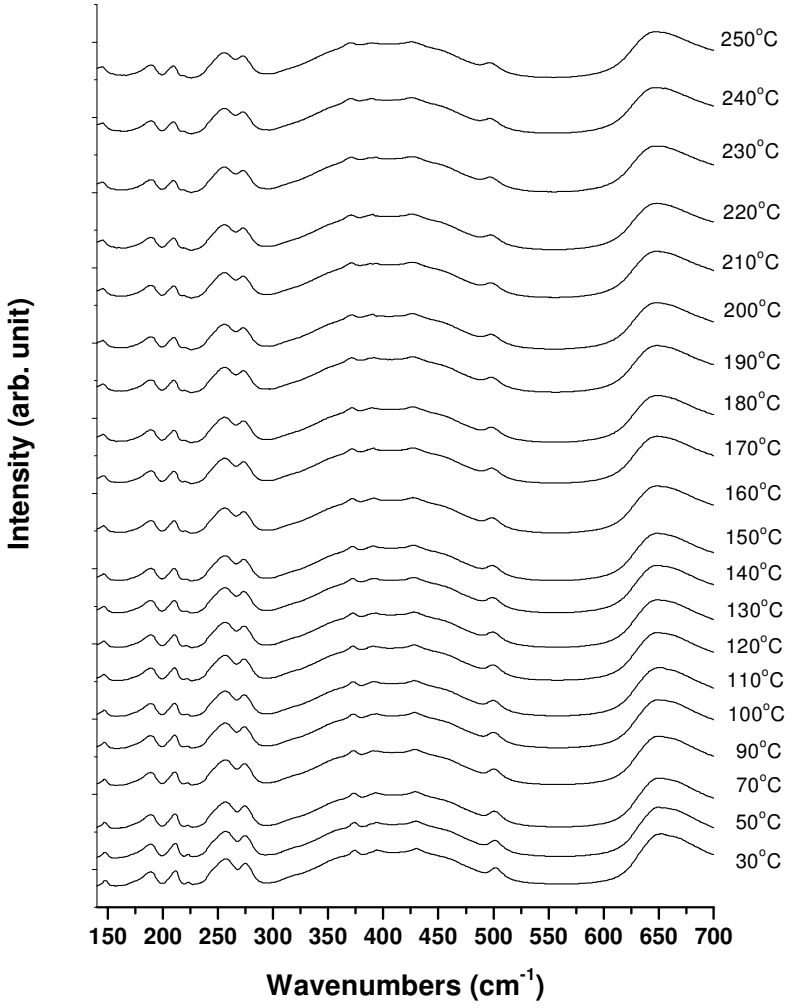
Intensity (arb. unit)
250°C
240°C
230°C
220°C
210°C
200°C
190°C
180°C
170°C
160°C
150°C
140°C
130°C
120°C
110°C
100°C
90°C
70°C
50°C
30°C
150 200 250 300 350 400 450 500 550 600 650 700
Wavenumbers (cm-1)

Fig 7

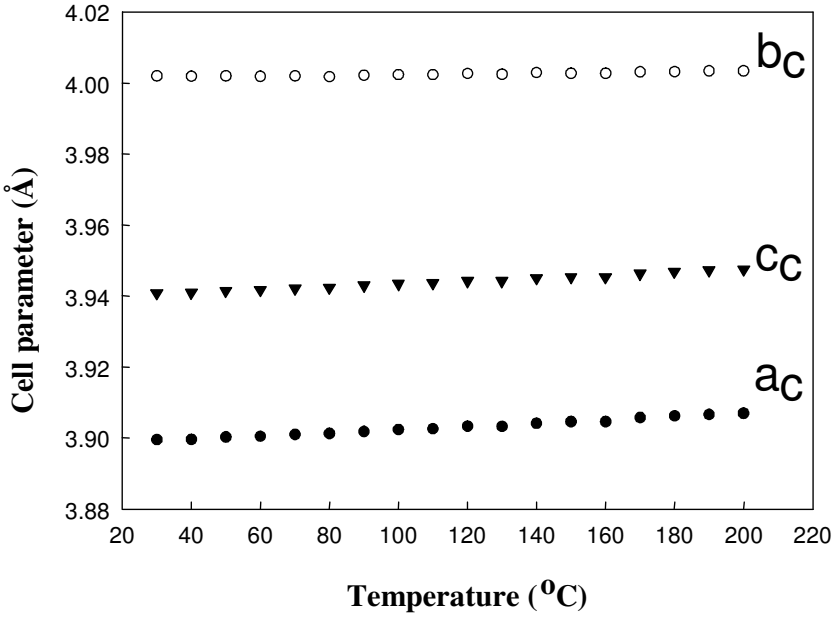
4.02
4.00
3.98
3.96
3.94
3.92
3.90
3.88
Cell parameter (Å)
20
40
60
80
100
120
140
160
180
200
220
Temperature (°C)
bc
cc
ac

Fig. 8